

## Statistical and dynamic models of charge balance functions

Sen Cheng,<sup>\*</sup> Silvio Petriconi, Scott Pratt, and Michael Skoby<sup>†</sup>

*Department of Physics and Astronomy and National Superconducting Cyclotron Laboratory, Michigan State University, East Lansing, Michigan 48824, USA*

Charles Gale, Sangyong Jeon, Vasile Topor Pop, and Qing-Hui Zhang

*Physics Department, McGill University, Montréal, Québec, H3A 2T8 Canada*

(Received 30 December 2003; published 28 May 2004)

Charge balance functions, which identify balancing particle-antiparticle pairs on a statistical basis, have been shown to be sensitive to whether hadronization is delayed by several fm/c in relativistic heavy ion collisions. Results from two classes of models are presented here, microscopic hadronic models and thermal models. The microscopic models give results which are contrary to recently published  $\pi^+\pi^-$  balance functions from the STAR Collaboration, whereas the thermal model roughly reproduces the experimental results. This suggests that charge conservation is local at breakup, which is in line with expectations for a delayed hadronization. Predictions are also presented for balance functions binned as a function of  $Q_{\text{inv}}$ .

DOI: 10.1103/PhysRevC.69.054906

PACS number(s): 25.75.Gz

### I. INTRODUCTION

Energy densities of near 10 GeV/fm<sup>3</sup> covering volumes of several hundred fm<sup>3</sup> are attained in Au+Au collisions at the Relativistic Heavy Ion Collider (RHIC). Given that the volume of a typical hadron is approximately 1 fm<sup>3</sup>, this far exceeds the energy density of a typical hadron. Therefore, quark and gluon degrees of freedom are expected to provide a meaningful basis for describing the microscopic motion for several fm/c, until the matter expands and cools to a point where hadronic degrees of freedom again become appropriate.

The conversion from partonic to hadronic degrees of freedom should be accompanied by a large increase in the number of quark-antiquark pairs as the entropy stored in gluons and quarks is converted to hadrons, each of which has at least two quarks. These newly created charges are significantly more correlated to their balancing anticharges than those charge pairs created in the early stages of the collision. In fact, these newly created pairs should be more tightly correlated than pairs from  $pp$  collisions. In  $pp$  collisions, most pairs are created within the first 1 fm/c in the decay of color flux tubes, or strings, which involves the separation of the balancing quarks through tunneling. If the quarks separate by a distance of 0.5 fm at a time of 0.5 fm/c, they find themselves in regions where the collective rapidities differ by one unit since the velocity gradient along the beam axis is approximately  $1/\tau$ . In contrast, a quark that is produced at 5 fm/c and is 0.5 fm from its balancing partner is separated by only one-tenth of a unit of rapidity. Thus, a measurement of the relative separation of balancing charges would yield

invaluable information concerning whether hadronization was delayed beyond the characteristic hadronic time scale of 1 fm/c [1].

Charge balance functions provide the means to identify balancing charges on a statistical basis through a like-sign subtraction. The balance function is defined as a conditional distribution,

$$B(P_2|P_1) \equiv \frac{1}{2} \left\{ \frac{N_{+-}(P_1, P_2) - N_{++}(P_1, P_2)}{N_+(P_1)} + \frac{N_{-+}(P_1, P_2) - N_{--}(P_1, P_2)}{N_-(P_1)} \right\}, \quad (1)$$

where the  $+/-$  indices refer to particles or antiparticles. Expressed in words, the balance function measures the probability of observing an extra particle of the opposite sign with momentum  $P_2$  given the observation of the first particle with momentum  $P_1$ . Typically,  $P_1$  will refer to a particle observed anywhere in the detector, and  $P_2$  will refer to either the relative rapidity  $\Delta y$  or the relative momentum  $Q_{\text{inv}}$ . In such a case, the balance function is then labeled by only one variable, e.g.,  $B(\Delta y)$ .

The STAR Collaboration has recently published the first measurement of charge balance functions in relativistic heavy ions [2]. Measurements were performed for all charged particles as a function of the relative pseudorapidity and as a function of relative rapidity for identified pions. Indeed, the presence of the extra balancing charges was apparent and statistics were sufficient to make distributions as a function of the relative rapidity as illustrated in Fig. 1. Remarkably, the width of the balance function in  $\Delta y$  decreased with the centrality of the collision, qualitatively consistent with expectations for an increasingly delayed hadronization as shown in Fig. 2.

The purpose of this paper is to compare the behavior seen by STAR with two classes of calculations. First, we compare to two microscopic hadronic simulations, RQMD [3] and

<sup>\*</sup>Present address: Sloan-Swartz Center, University of California at San Francisco, 513 Parnassus Avenue, Box 0444, San Francisco, CA 94143-0444, USA.

<sup>†</sup>Present address: Department of Physics, Purdue University, 525 Northwestern Avenue, West Lafayette, IN 47907, USA.

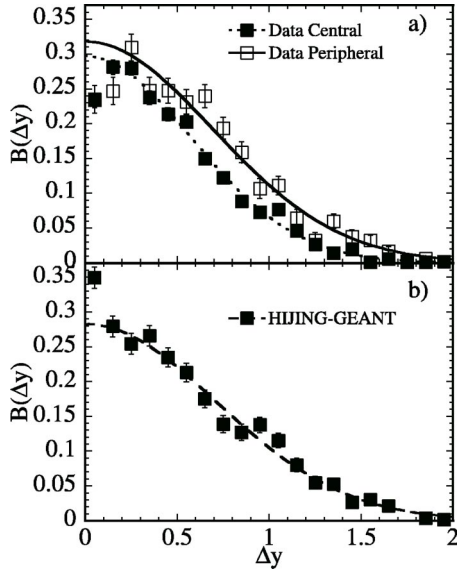


FIG. 1. Balance functions for charged pion pairs as measured by the STAR Collaboration. For each charged pion, there is an enhanced probability of finding an extra charged pion of the opposite sign within a unit of rapidity. The peripheral data are well reproduced by the HIJING model, which can be considered as being caused by overlapping independent  $pp$  collisions.

HIJING/GROMIT [4,5]. Both approaches involve creating the bulk of hadrons instantaneously according to  $pp$  phenomenology with the subsequent rescattering modeled by a hadronic cascade. As will be seen in Sec. II these models give qualitatively different behavior than what was observed by STAR, i.e., the width of the balance functions increases with the centrality of the collision rather than decreases. Sections III–V present the formulation and results of a thermal model that inserts charge conservation into the blast-wave model which has been successful in describing spectra. In this model an ensemble of particles is simulated from a single thermal domain in such a way that the net baryon number, electric charge, and strangeness are zero. These particles then have their momenta and space-time coordinates reassigned

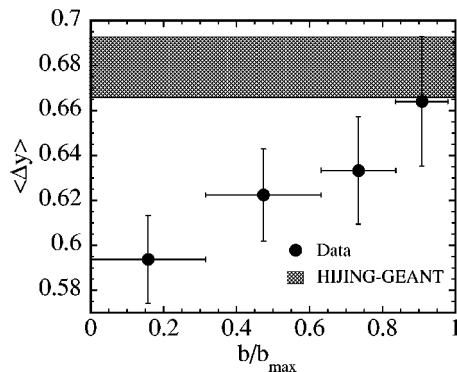


FIG. 2. The mean widths of  $\pi^+\pi^-$  balance functions as measured by STAR. For small impact parameters  $b$ , the balance function becomes narrower, qualitatively consistent with expectations for a quark-gluon plasma. For peripheral collisions, the width matches predictions from HIJING.

according to a blast-wave prescription. The effect of interdomain interactions, which were shown to be non-negligible in [6], is also taken into account and described in Sec. IV. The resulting balance functions are in remarkable agreement with the STAR measurement provided the domain is constrained to being highly localized in coordinate space, as would be expected in the delayed-hadronization scenario. The final section presents an interpretation of this comparison and presents a discussion of the prospects for making similar comparisons with  $K^+K^-$  or  $p\bar{p}$  balance functions.

## II. BALANCE FUNCTIONS FROM MICROSCOPIC HADRONIC SIMULATIONS

One fm/c after the initial collision the energy densities achieved in Au+Au collisions at the RHIC are in the neighborhood of 5–10 GeV/fm<sup>3</sup> [7]. In hadronic simulations, hadrons are generated from overlapping nucleon-nucleon simulations with the creation times typically being less than 1 fm/c. Thus, such calculations simulate the evolution of the collision by assuming hadrons are formed and that they propagate in an environment that should preclude their very existence due to the high energy density. Despite the inherent inconsistency in these approaches, such calculations are important as they provide a baseline from which one can understand the degree to which novel degrees of freedom and collective phenomena alter the final state. Here, we present results from several such models. The first is RQMD [3] which has been the work horse of such models over the last decade. The second approach represents a merging of HIJING and a hadronic cascade GROMIT, which, like RQMD, models the final-state interactions through the scattering of the hadrons. This second approach is less sophisticated than RQMD, but has an advantage in speed, allowing the compilation of 20 000 central events. Comparisons with many of the same models have been performed for charge fluctuations [8], which are intimately related to balance functions [9].

For the purposes of this paper, the important aspect of the simulations is that they provide a model where the various charges are created early, experience numerous interactions, and are eventually emitted into the final state. In both RQMD and HIJING/GROMIT, the charges are created principally by the initial fragmentation of strings. Like other string-based microscopic models [3,10–13,15–18], these models incorporate a formation time of the scale of 1 fm/c. These approaches are significantly different from VNI/URQMD [19], where the initial stage of the collision is dominated by a partonic (mostly gluonic) cascade. In the string-based models, the created charges are typically separated along the beam axis by a distance characterized by a 1 fm scale. It is convenient to monitor the particle spatial position along the beam axis with the coordinate  $\eta$ ,

$$\eta = \frac{1}{2} \log \left( \frac{t+z}{t-z} \right), \quad (2)$$

where for small distances,

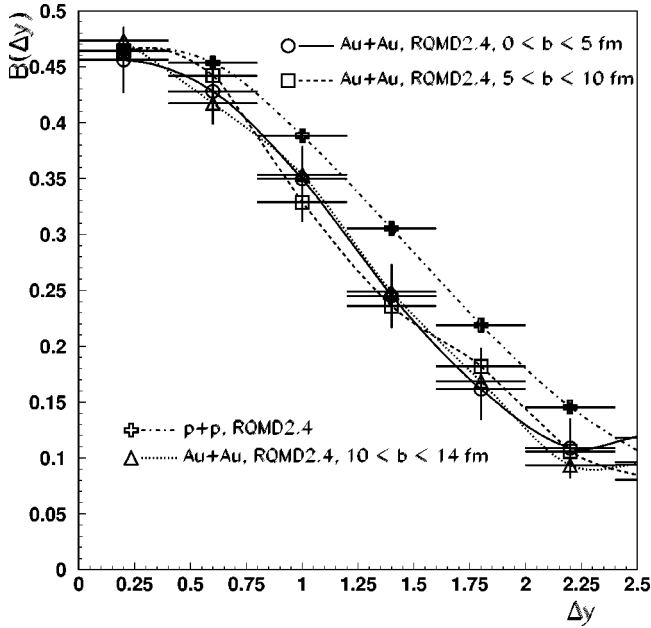


FIG. 3.  $\pi^+\pi^-$  balance functions for RQMD are shown for both  $pp$  and Au+Au collisions assuming a perfect detector. In contrast to the experimental results of [2], the balance function is slightly broader for central Au+Au collisions.

$$\Delta\eta = \Delta z / \tau. \quad (3)$$

In string models, as well as in boost-invariant hydrodynamics,  $\eta$  is tightly correlated to the collective rapidity of the surrounding particles, i.e.,  $y_{\text{collective}} \approx \eta$ . If a pair is created at  $\tau \sim 1$  fm/c and is separated by nearly 1 fm, the separation in  $\eta$  at this time is approximately one unit. Thus, the two particles reside in regions which have a collective rapidity difference of approximately one unit and they will be swept apart from one another by the collective flow. Reinteraction provides only a diffusive contribution which further broadens the separation in  $\eta$ .

Figure 3 displays  $\pi^+\pi^-$  balance functions from RQMD. Due to a lack of statistics, calculations were performed assuming a perfect detector. Results are shown for both  $pp$  collisions and for Au+Au collisions. Although the statistics

are marginal, the balance function does appear a few percent wider for Au+Au as compared to peripheral Au+Au. This is in contrast to the data which show the balance function narrowing by approximately 15%. The results of Fig. 3 are summarized in Table I. The half-widths were calculated by fitting the balance functions to a Gaussian form, similarly to what was done in [2]. Results are also shown for HIJING and HIJING  $B/\bar{B}$  [14] which incorporate different string prescriptions than RQMD and ignore rescattering. As shown in [2] the widths from HIJING do not change from Au+Au to  $pp$  as expected.

Table I also provides the  $\chi^2$  per degree of freedom from the Gaussian fit. The discrepancy between the shape of the balance function and a Gaussian is especially apparent for the calculations for  $pp$  collisions which were performed with a large event sample of 40 000 events. Unfortunately, similar statistics were not attained for the other calculations.

Similar results were obtained with the HIJING/GROMIT treatment as can be seen in the lower panel of Fig. 4. Since the statistics are improved relative to the RQMD calculation, a simplified version of the STAR acceptance was taken into account. Pseudorapidities were confined to midrapidity,  $|\eta| < 1.1$ , transverse momenta were required to be greater than 100 MeV/c, and the magnitude of the momenta was confined to be less than 700 MeV/c. In this case, both curves represent Au+Au collisions, but in one case the reinteraction has been ignored. As with RQMD, the inclusion of hadronic scatterings appears to marginally broaden the balance function.

The upper panel of Fig. 4 shows analogous results from GROMIT/HIJING binned in  $Q_{\text{inv}}$  rather than the relative rapidity. Here, the balance function is slightly narrower after the inclusion of reinteractions. The difference of the  $Q_{\text{inv}}$  and  $\Delta y$  binnings derives from two effects. First, during the reinteraction stage, the matter cools, which reduces the thermal contribution to the width of the balance function. The cooling affects all three dimensions of relative momenta. Secondly, the mean  $p_t$  decreases due to loss of transverse energy that accompanies the longitudinal expansion. Since the relative rapidity is related to the relative momentum via  $Q_{\text{long}} \sim m_T \Delta y$ , where  $m_T$  is the transverse mass, a reduction of the average transverse mass will result in a narrower balance function when plotted as a function of  $Q$  when the width of

TABLE I. Half-widths of balance functions calculated with RQMD, HIJING, and HIJING  $B/\bar{B}$ . Experimental acceptance was not taken into account for these calculations.

Model	$b$ (fm)	Half-width	$\chi^2$ per degree of freedom
RQMD (AuAu)	0–3	$1.56 \pm 0.11$	1.16
RQMD (AuAu)	3–5	$1.42 \pm 0.11$	1.1
RQMD (AuAu)	5–7	$1.41 \pm 0.11$	2.0
RQMD (AuAu)	7–10	$1.39 \pm 0.11$	2.9
RQMD (AuAu)	10–14	$1.32 \pm 0.11$	1.0
RQMD (pp)		$1.48 \pm 0.11$	5.49
HIJING (AuAu)	0–3	$1.14 \pm 0.11$	0.92
HIJ/ $\bar{B}$ (AuAu)	0–3	$1.24 \pm 0.08$	0.55
HIJING (pp)		$1.18 \pm 0.02$	5.51

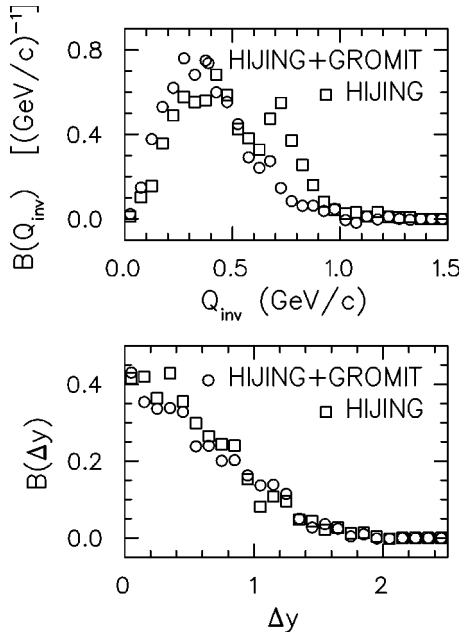


FIG. 4. Balance functions for HIJING with and without the hadronic cascade GROMIT are shown as a function of the rapidity difference in the upper panel and as a function of  $Q_{inv}$  in the lower panel. These results have incorporated the STAR acceptance, but not the efficiency. The incorporation of the cascade leads to a slightly broadened balance function when analyzed as a function of  $\Delta y$  and a narrower balance function when analyzed as a function of  $Q_{inv}$ . This apparent contradiction derives from the failure of HIJING/GROMIT to correctly describe the dependence of  $\langle p_t \rangle$  as a function of centrality.

the balance function in relative rapidity is unchanged. Thus, part of the discrepancy between GROMIT/HIJING and data can be attributed to the failure to describe the behavior of the mean transverse mass as a function of centrality, which increases by  $\sim 10\%$  for central collisions in experiment. As described in [6], failure caused by a model not fitting the  $p_t$  spectra vs failure stemming from not describing the dynamics of charge balance can be better distinguished by analyzing the balance functions in  $Q_{inv}$ , or better yet,  $Q_{out}$ ,  $Q_{side}$ , and  $Q_{long}$ .

Another striking aspect of Fig. 4 is the disappearance of the  $\rho$  peak for  $Q_{inv}$  near  $700 \text{ MeV}/c$ . This is also a natural consequence of cooling which lowers the  $\rho/\pi$  ratio as the temperature falls to near  $100 \text{ MeV}$  near breakup.

### III. THE CANONICAL BLAST-WAVE MODEL

One of the most notable results from the first two years of RHIC data is the success of the blast-wave model in describing spectra, particle yields, and correlations. The blast-wave model provides an especially important benchmark for balance functions. Assuming that emission from the final state has a thermal character, the narrowest balance function would constrain charges and their balancing partners to be emitted from identical space-time regions. The width of the balance function would then be determined principally by the breakup temperature, and to a lesser degree by the reso-

nance composition [20]. If the evolution of the reaction was characterized by an expanding chargeless long-lived gluonic mire which hadronized close to the breakup, it would be natural to confine particles and their balancing charges to be emitted in close proximity. Relaxing this constraint by incorporating nonzero correlation lengths can only broaden the balance function [6].

Since charge conservation is local, and since the charge does not have time to mix throughout the entire collision volume, one needs to choose a volume for performing the canonical calculations. This scale should be determined by the distance charge might diffuse by the time the system has reached chemical freeze-out. We refer to each of these subvolumes as a domain and view the entire system as a collection of independent domains.

Of the numerous variations of the blast-wave model [21–25], we employ a simplified version of this model, where emission occurs at a single proper time from thermal sources moving with a linear velocity profile. The model is characterized by a kinetic freeze-out temperature  $T_k$ , a chemical freeze-out temperature  $T_\mu$ , the velocity at the edge  $v_{max}$ , and the maximum radius  $R$ . The extent along the beam direction is assumed to be infinite and the distribution of domains is assumed to be uniform in the transverse direction.

$$\frac{dN}{rdr} = \begin{cases} \text{const}, & r < R, \\ 0, & r > R. \end{cases} \quad (4)$$

The transverse rapidity of domains,  $y_{t,\text{domain}}$ , is assumed to follow the position  $r$ :

$$y_{t,\text{domain}} = y_{t,\text{max}} \frac{r}{R}. \quad (5)$$

The longitudinal rapidity of the domain,  $y_{\text{domain}}$ , is chosen randomly within  $\pm 3$  units of zero. Since thermal rapidities are on the order of one to two units, this effectively represents a boost-invariant source. For this study, we assume that every particle in a given domain is emitted from a thermal source moving with the velocity of that domain. If the domain has a significant spatial extent in the beam direction, the source rapidities would be spread around the domain rapidity by a finite amount which would broaden  $B(\Delta y)$  [6]. Thus, the balance functions shown here represent the narrowest possible result for a thermal model. The only way to provide further significant narrowing would be to lower the breakup temperature, which would require a corresponding increase in the transverse collective flow.

The simplest model of each source would be that of particle/antiparticle pairs, i.e., each  $\pi^+$  would be balanced by a  $\pi^-$  and each  $K^+$  would be balanced by a  $K^-$ . However, charge mixing and chemical equilibration spreads the balancing of charge among multiple constituents. For instance the electric charge and strangeness of a  $K^+$  might be balanced by a  $\bar{p}$  and a  $\Lambda$ . To account for these effects, we generate all the particles from a source in a manner which is consistent with the canonical ensemble. The chemical composition of each source will be governed by a volume  $V_\mu$ , a temperature  $T_\mu$ , and the constraint of zero net projection  $I_3$ , and baryon number. After generating the particles with  $T_\mu = 175 \text{ MeV}$ , the

particles will have their momenta reassigned according to the blast-wave prescription mentioned above with a breakup temperature,  $T_k = 120$  MeV, and a maximum transverse flow velocity of  $0.7c$ . The particles are given coordinates corresponding to the position of the domain and are then boosted by the domain velocity. Mesons were chosen from the flavor octet and singlet ground state pseudoscalars and pseudovectors, while baryons were chosen from the ground state baryon decuplet and octet. The particles were then decayed according to measured decay rates and branching ratios [26].

In order to perform the Monte Carlo generation of particles from a given thermal source, one must first calculate the canonical partition functions for a fixed charge  $\vec{Q}$  and a fixed number  $A$ . This is accomplished by employing recursion relations, which have been applied to a variety of problems in nuclear statistical physics where charge and symmetry constraints play an important role. These applications include multifragmentation [27–29], nuclear level densities [30], isospin distributions for pions [31], and a parton gas confined to a color singlet [32]. For the calculations presented here, Bose and Fermi effects will be neglected and only additive charges will be considered. This results in a straightforward recursion relation for the partition function.

$$Z_{A,\vec{Q}}(T,V) = \sum_k \frac{a_k}{A} \omega_k(T,V) Z_{A-a_k,\vec{Q}-\vec{q}_k}(T,V), \quad (6)$$

where  $k$  labels the particular species, e.g.,  $\pi^+$ ,  $\pi^0$ ,  $p$ ,  $\Delta^{++}$ . The partition function of a single particle of type  $k$  is  $\omega_k$ . The number  $A$  counts the sum,  $\sum_k a_k$ , where  $a_k$  can be any positive integer. Since the method will consider all  $A$ , the choice of  $a_k$  is arbitrary. We choose  $a_k$  to be unity for all stable particles and to equal two for unstable particles.

Generating a set of particles from one domain is performed with the following steps: (1) Generate the partition function,  $Z_{A,\vec{Q}}(T,V)$  for all  $A$  and  $\vec{Q}$ . (2) Choose a number of hadrons,  $A$ , proportional to the weight  $Z_{A,\vec{Q}=0}$ . (3) Choose a species  $k$  proportional to the weight  $\omega_k Z_{A-1,\vec{Q}-\vec{q}_k} / Z_{A,\vec{Q}}$ . (4) Return to step 2 after replacing  $A \rightarrow A - a_k$ ,  $\vec{Q} \rightarrow \vec{Q} - \vec{q}_k$ . This procedure naturally ends when  $A = \vec{Q} = 0$ . Since particles from one domain are uncorrelated with particles from another domain, the balance function need only sum over pairs from the same domain.

To prove that this prescription is consistent with the partition function, one must show that there is an equivalence between the partition function and a sum over weights of independent ordered paths. Each path  $\mathcal{P}(A,\vec{Q};n,k_1 \cdots k_n)$  is an ordered list of  $n$  particles,  $k_1 \cdots k_n$  which sums to the correct  $A$  and  $\vec{Q}$ . One can then assign a weight for each path,

$$w(A,\vec{Q};n,k_1 \cdots k_n) \equiv \prod_{i=1}^n \omega_{k_i} \frac{a_{k_n}}{\sum_{i \leq n} a_{k_i}}. \quad (7)$$

One can then define  $\Omega(A,\vec{Q})$  as the sum over such paths that yield  $A$  and  $\vec{Q}$ :

$$\Omega(A,\vec{Q}) \equiv \sum_{n,k_1 \cdots k_n, \text{ such that } \sum a_{k_i} = A, \sum \vec{q}_{k_i} = \vec{Q}} w(A,\vec{Q},k_1 \cdots k_n). \quad (8)$$

Since the contribution from each path is a product, and since the last term can be written in terms of  $A$ ,  $\vec{Q}$  and the properties of  $k_n$ , one can write a recursion relation for  $\Omega(A,\vec{Q})$  by factoring the last term,

$$\Omega(A,\vec{Q}) = \sum_{k_n} \frac{a_{k_n}}{A} \omega_{k_n} \Omega(A - a_{k_n}, \vec{Q} - \vec{q}_{k_n}, k_1 \cdots k_n), \quad (9)$$

which is the same recursion relation used for the partition function. Furthermore, since  $\Omega(A=0) = Z(A=0) = 1$ ,  $\Omega$  and the partition function  $Z$  are identical. Once the partition function can be identified as a sum over weights of independent paths, one can justify the Monte Carlo procedure outlined above.

Since charge conservation is enforced on a domain-by-domain basis, there are no inter-domain contributions to the balance function from this procedure. This greatly accelerates calculation as one need only consider pairs from within the same domain when calculating the distributions  $N_{+ \cdots}$  used to construct the balance function.

The resulting balance functions are only sensitive to the choice of domain volume if the volumes are near or below a few dozen  $\text{fm}^3$ . For the calculations presented later in this paper, the volume was chosen to be  $64 \text{ fm}^3$ . This would imply, that at the point where chemical freeze out occurs, charge conservation is enforced on a length scale of  $\sim 4 \text{ fm}$ . If one were to choose a much smaller volume, the likelihood that the charge of a  $\pi^+$  would be balanced by a  $\pi^-$ , vs the likelihood of being balanced by an assortment of other particles, would be increased by several percent. This would result in a larger normalization for the  $\pi^+ \pi^-$  balance function.

#### IV. INTERDOMAIN CORRELATIONS

The philosophy of the balance function is predicated on the assumption that the background subtraction in the balance function's numerator will statistically isolate balancing pairs. Of course, one must consider the spread of the balancing charge among other hadrons in the same domain. This was taken into account with the Monte Carlo procedure outlined in the previous section. This procedure accounts for strong interactions between neighbors, but only those resonant interactions included in the list of particles. For example, the interaction  $\pi^+ \pi^- \leftrightarrow \rho^0$  would be included by incorporating the  $\rho^0$  into the resonance list. Given that resonances alter the shape of the balance function at the 10% level, and that two-particle phase shifts are largely driven by resonant interactions, this procedure should crudely account for the strong interaction between neighbors.

Unfortunately, the procedure thus far does not account for the Coulomb interaction which was shown to be non-negligible in [6]. The method also ignores nonresonant strong interactions between neighbors and correlations from

identical-particle interference. The long-range Coulomb interaction is especially important as it extends beyond the particle's neighbors to those particles generated in separate domains. A charged particle will effectively polarize other pairs increasing the likelihood that a particle of opposite charge is emitted at smaller relative momentum than the balancing charge. This results in an enhancement to the balance function at relative momenta less than a few hundred MeV/ $c$  and a suppression at larger relative momentum. Nonresonant strong interactions can also affect the balance function since they provide a correlation between like-sign pairs that is different from the correlation they induce between unlike-sign pairs. Finally, identical-particle interference can affect balance functions by increasing the probability that two charges of the same sign have small relative momentum. This results in a hole in the balance function for relative momenta below  $\sim 100$  MeV/ $c$ . However, the Coulomb again dominates at very low relative momentum and a sharp peak is expected for relative momenta near or below 10 MeV/ $c$ . Since the Coulomb interaction is long range, interdomain correlations from Coulomb interactions increase with the centrality of the collisions because a given particle will be correlated with an increasing number of other particles as the multiplicity of the collision is increased. Correlations from short-range interactions should be less sensitive to the multiplicity since the number of neighbors depends principally on the breakup density rather than the system size. The distortion from identical-boson interference will be confined to a decreasing range of relative momentum as the system size increases. However, since there is an increasing number of particles per element of momentum, the magnitude of the distortion increases with centrality while the range of the distortion shrinks.

In [6] the interdomain correlation was modeled by generating two pairs of particles  $a_1, a_2$  and  $b_1, b_2$ . The particles  $a_1$  and  $a_2$  were antiparticle reflections of one another, as were the particles  $b_1$  and  $b_2$ . In the limit of small domains, where the multiplicity of a domain is never more than 2, this is equivalent to the present problem. The effects of the interdomain Coulomb force was included by calculating a correlation weight formed by the product of all two-particle interdomain correlation functions,  $W_{AB} = C_{a_1, b_1}(p_{a_1}, p_{b_1}) C_{a_1, b_2}(p_{a_1}, p_{b_2}) C_{a_2, b_1}(p_{a_2}, p_{b_1}) C_{a_2, b_2}(p_{a_2}, p_{b_2})$ . Each two-particle correlation function was generated from a simple Gaussian source functions. For each set of pairs the weight was applied to all the distributions  $N_{++}, N_{+-}, \dots$  used to calculate the balance function numerators as well as the one-particle distributions  $N_+$  and  $N_-$  used to form the balance-function denominators. For each  $ab$  pair, the number of  $cd$  pairs sampled was chosen to achieve consistency with the experimental multiplicity.

The method of [6] has two shortcomings. First, the product ignored correlations of correlations. For instance, the product  $C_{ac} C_{ad}$  neglects the fact that, if  $a$  and  $c$  are correlated, then they are more likely to have been close to one another in coordinate space; therefore  $a$  and  $d$  would more likely be close to one another since  $c$  and  $d$  are from the same domain. The more obvious limitation of this approach is that it cannot handle the chance that the domain consists of several dozen particles, with the constraint of charge conservation being spread throughout the domain.

The first shortcoming can be accounted for by replacing the product of correlation functions with a product of squared wave functions,

$$W_{AB} = \left\langle \prod_{a \in A, b \in B} |\phi_{ab}(p_a - p_b, x_a - x_b)|^2 \right\rangle. \quad (10)$$

Here,  $\phi_{ab}$  is the relative wave function for an outgoing plane wave with asymptotic relative momentum  $p_a - p_b$ , and the averaging covers the distribution of source points  $x_a$  and  $x_b$ . If the expectation of the products of the squared wave function were replaced by the product of expectations, Eq. (10) would become the product of correlation functions, and would be equivalent to the method of [6] in the case where each domain had two particles.

The pairs were generated according to the blast-wave prescription described in the previous section, with both particles from a given pair being assigned the same point in coordinate space. Balance-function numerators were then calculated using only the two pairs, and ignoring the contribution where both particles originate from the same pair. Rather than incrementing a bin by unity when an appropriate pair is found, the quantities  $N_{++}$  and  $N_{+-}$  were incremented by  $W_{AB}$ . Since the source of the pairs was confined to a region of  $-\eta_{\max} < \eta < \eta_{\max}$  where  $\eta_{\max} = 2$ , the balance function is then scaled upward by a factor of the number of pion pairs which should be emitted within the central four units of rapidity. For the calculations in this paper it was assumed that the number of pairs would be 200 per unit rapidity.

For a perfect detector, the weight  $W_{AB}$  is added to both  $N_{++}$  and  $N_{+-}$ . Thus, the normalization for the balance function is unchanged by interdomain correlations, i.e., the interpair interactions effectively polarize the pairs but they do not enhance the overall number of one charge vs another. This constraint is relaxed after detector acceptance is taken into account.

We believe that this estimate of the distortion from interpair correlations can only be trusted at the 20% level. First, some of the pions are emitted from long-lived resonances and should not contribute. Accounting for these effect should reduce the effect by several tens of percent. Other aspects of the approximation, such as neglecting interactions with other particles and requiring both particles from a given pair to originate from the same point, may also affect the answer at the 10% level.

Wave functions for a pair  $ab$  were calculated using full Coulomb wave functions. As only  $\pi^+ \pi^-$  correlations are being considered here, the wave functions were symmetrized only if  $a$  and  $b$  were identical pions. Strong interaction corrections were also only applied if  $a$  and  $b$  were pions. The wave functions were modified by the strong interaction using the methods of Ref. [33]. In [33] the wave functions for  $|\mathbf{x}_1 - \mathbf{x}_2| > 1$  fm were calculated using phase shifted partial waves, while effective squared wave functions were applied for small distances. These effective forms were also completely determined by the phase shifts. The phase shifts for  $\pi^+ \pi^-$  were taken from experiment whenever possible. Unfortunately, they are not well understood for invariant masses above the two-kaon threshold.

The dominant phase shift is in the  $\ell=1, I=1$  channel which is driven by the  $\rho$  resonance. A Breit-Wigner function was applied for this channel:

$$\tan \delta = \frac{\Pi_I}{M_0^2 - M^2}, \quad (11)$$

$$\Pi_I = \Pi_{I,0} \frac{M_0}{M} \left( \frac{q}{q_0} \right)^3 F(q, q_0), \quad (12)$$

$$\Pi_{I,0} = \Gamma_0 M_0. \quad (13)$$

The  $\ell=0, I=0$  channel also plays an important role in affecting the wave function. Although phase shift analyses do not reveal a sharp peak as in a resonance [34–38], the phase shifts are considerable, rising steadily from zero at threshold to approximately  $90^\circ$  at  $M=2M_K \sim 1$  GeV, where the kaon channel opens. At the two-kaon threshold, the behavior of the phase shifts becomes complicated and an inelastic treatment becomes warranted. Since one uses derivatives of the phase shifts to find the density of states, interpolating data for phase shifts can be dangerous due to noise in the experimentally determined phase shifts. Thus, we apply a simple form that describes the general behavior,

$$\tan(\delta_{I=0, \ell=0}) = \frac{aq}{1 - (q/a_2) + (q^2/a_3^2)}, \quad (14)$$

$$a = 0.204/m_\pi, \quad a_2 = 290 \text{ MeV}/c, \quad a_3 = 625 \text{ MeV}/c. \quad (15)$$

The coefficient  $a$  is chosen to reproduce the scattering length, which is small due to constraints from chiral symmetry [34,39]. The remainder of the denominator is chosen to provide crude agreement with measured phase shifts up to invariant masses of 1 GeV. Since the phase shift rises only half as high as the  $I=1, \ell=0$  phase shift, and since it contributes only one-third as much from a lower spin degeneracy, this channel has a fairly marginal impact on the wave functions.

Other phase shifts also contribute: ( $I=2, \ell=0$ ), ( $I=0, \ell=2$ ), and ( $I=2, \ell=2$ ). Since none of these phase shifts exceed more than a few degrees, they make nearly negligible contributions to the density of states. For the ( $I=2, \ell=0$ ) channel, we apply an effective range expansion [40],

$$\tan \delta = \frac{qa}{1 + aq^2 R_{\text{eff}}/2}, \quad (16)$$

$$a = -0.13 \text{ (MeV}/c)^{-1}, \quad R_{\text{eff}} = 1.0 \text{ fm}. \quad (17)$$

For the ( $I=0, \ell=2$ ) phase shift, the data [41] are rough, and we make a simple expansion,

$$\tan(\delta_{I=0, \ell=2}) = ax^5, \quad x = \frac{q}{1 + q^2/\Lambda^2}, \quad (18)$$

where  $a=6.2 \text{ GeV}^{-1}$ ,  $\Lambda=1 \text{ GeV}/c$ . For the ( $I=2, \ell=2$ ) partial wave, we use the same expansion [40] with the parameters  $a=8.4 \text{ GeV}^{-1}$  and  $\Lambda=0.4 \text{ GeV}/c$ . Although none of the last three channels is particularly well understood, it is clear

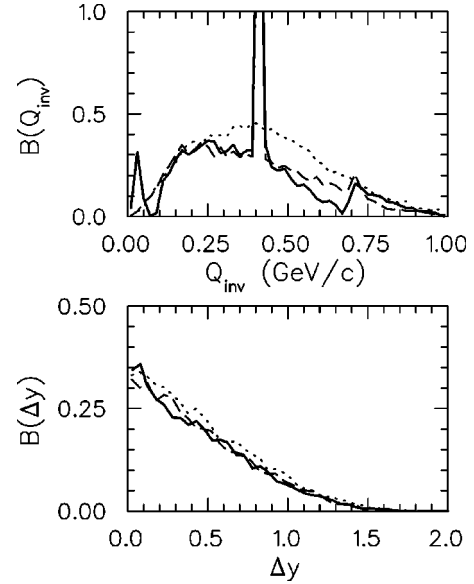


FIG. 5. Balance function results for a pion gas (dotted lines) and for a resonance gas (dashed lines) are shown for the canonical thermal blast-wave model. Resonances clearly narrow the balance function when plotted against  $Q_{\text{inv}}$  (upper panel) but have little effect on the balance function when plotted as a function of the rapidity difference (lower panel). Balance functions corrected for interpair correlations (solid lines) again differ when plotted as a function of  $Q_{\text{inv}}$ . The additional distortion arises from the effects of Coulomb interaction, symmetrization, and a more sophisticated treatment of the strong interaction.

they do not have a substantial impact on the result.

## V. CANONICAL BLAST WAVE RESULTS

Calculations for the canonical blast-wave calculations described in Sec. III and Sec. IV were performed assuming a temperature of  $T_k=120$  MeV and a maximum transverse velocity of  $0.7c$  to provide crude agreement with spectra. The transverse radius was chosen to equal 13 fm and the breakup time  $\tau$  was chosen to be  $10 \text{ fm}/c$  to reproduce HBT results. The chemical composition was governed by a temperature  $T_\mu=175$  MeV as suggested by fits of the particle yields [42].

Figure 5 displays results for balance functions analyzed in both  $\Delta y$  and  $Q_{\text{inv}}$ . The acceptance and efficiency of the STAR detector have been applied to the calculation of the distributions that are used to construct the balance function. These accepted particles include products of weak decays of strange baryons and  $K_s$  mesons. Results are shown both with and without the contribution from interdomain correlations. Since the interaction of  $\pi^+ \pi^-$  pairs through the  $\rho^0$  meson was incorporated into the relative wave functions, the contribution from  $\rho^0$ 's were eliminated before the interdomain correlations were added.

The relative contribution of resonances and strong interactions can be estimated by considering the chance that a charged pion originated from a resonance that also produced a pion of the opposite charge. Although such estimates suggest contributions on the level of 10–20 %, they seem less

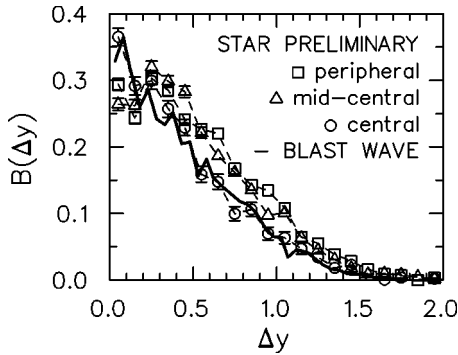


FIG. 6. Balance functions from 200A GeV Au+Au collisions measured by STAR are compared to the canonical blast-wave model described in the text. The model should set a lower bound for the width of a balance function provided the particles are emitted thermally. The remarkable agreement with the data suggests that charge conservation remains highly localized at breakup.

visible when viewing the results. This is because the separation of a  $\pi^+\pi^-$  pair in momentum is not much different coming from a resonance as compared to a distribution governed by two Boltzmann terms. In fact, the largest interdomain effect derives from the Coulomb interaction which moves some of the strength of the balance function to smaller relative momentum.

An absolute comparison with STAR results is displayed in Fig. 6. Both the height and width of the correlation are remarkably well matched by the thermal model. Since the canonical blast-wave calculation assumed the balancing charges were always emitted from sources moving with the same velocities, this represents the narrowest possible balance function one can generate with a final breakup temperature of 120 MeV. This appears to corroborate the scenario of late-stage hadronization, i.e., the existence of the quark-gluon plasma.

Before claiming that Fig. 6 provides “proof” of delayed hadronization, it is important to list a few qualifiers. First, the breakup temperature might be lower than the 120 MeV assumed here. Some estimates of the breakup temperature are near 100 MeV [25], although after the inclusion of resonances the temperatures are usually closer to 120 MeV. It should be kept in mind that an anomalously high yield of light neutral hadrons, e.g.,  $\eta$  mesons, could result in a narrower balance functions. A lower temperature or high  $\eta$  yield would narrow the balance function and permit the incorporation of a finite spread in the domain size along the beam axis. In Ref. [6] it was shown that since the thermal and diffusive contributions add in quadrature, the diffusive contribution is negligible unless the charge separates in coordinate space by of the order of one-half unit of  $\Delta\eta = \Delta z/\tau$  or more.

## VI. SUMMARY

The observed narrowing of the balance function is both qualitatively and quantitatively consistent with the scenario

of delayed hadronization, which should result in the separation of balancing charges being determined primarily by the collective flow and temperature of the breakup stage. The experimental results were well fitted by a canonical blast-wave calculation assuming a temperature of 120 MeV and a maximum transverse collective velocity of  $0.7c$ . By lowering the breakup temperature and raising the collective flow in the model, one should still be able to describe the pion spectra while producing a balance function that is even narrower than that observed experimentally. This would then allow one to accommodate a significant longitudinal size for the charge conservation domains in the thermal model. This ambiguity would be clarified by a multidimensional analysis of the balance function in the relative momenta of the pions. If the charge production is indeed delayed, the width of the balance function should be the same for  $Q_{out}$ ,  $Q_{side}$ , and  $Q_{long}$  [6].

Furthermore, the observations are opposite to the behavior predicted by purely hadronic models which predict a modest broadening of the balance function as centrality is increased. Unfortunately, the width of the balance function in relative rapidity is significantly affected by both the final temperature and the collective flow of the matter. Since HIJING/GROMIT gives the wrong behavior for the mean  $p_t$  as centrality increases, some of the failure to describe the centrality dependence of the balance function might derive from the inability to reproduce spectra rather than an inability to correctly describe the mechanism for charge production. This ambiguity would also be resolved by a multidimensional analysis.

The measurement, analysis, and phenomenology of charge balance functions is in its nascent stage. Nonetheless, the first analysis of RHIC data already provide important limits for understanding the production and separation of balancing charges in central gold collisions. There is tremendous promise for this class of observable as it is extended to more dimensions and to more species, e.g.,  $\bar{p}p$  and  $K^+K^-$ . These more detailed analyses should then provide a fingerprint for making unambiguous statements concerning the production and dissipation of charge in collisions at the RHIC. Since delayed hadronization is synonymous with delayed production of charge, these measurements can address the fundamental question of whether a new phase of matter has been created at the RHIC.

## ACKNOWLEDGMENTS

The comparison with STAR data could not have been performed without the acceptance and efficiency codes generously provided by Manuel Calderon. This work was supported by the Natural Sciences and Engineering Research Council of Canada, le Fonds Nature et Technologies of Québec, by the U.S. National Science Foundation Grant No. PHY-02-45009, and by the U.S. Department of Energy Grant Nos. DE-FG02-03ER41259 and DE-AC02-98CH10886.

- [1] S.A. Bass, P. Danielewicz, and S. Pratt, Phys. Rev. Lett. **85**, 2689 (2000).
- [2] J. Adams *et al.*, Phys. Rev. Lett. **90**, 172301 (2003).
- [3] RQMD Collaboration, H. Sorge, H. Stöcker, and W. Greiner, Ann. Phys. (N.Y.) **192**, 266 (1989).
- [4] X.N. Wang and M. Gyulassy, Comput. Phys. Commun. **83**, 307 (1994).
- [5] S. Cheng, S. Pratt, P. Csizmadia, Y. Nara, D. Molnar, M. Gyulassy, S.E. Vance, and B. Zhang, Phys. Rev. C **65**, 024901 (2002).
- [6] S. Pratt and S. Cheng, Phys. Rev. C **68**, 014907 (2003).
- [7] K. Adcox *et al.*, Phys. Rev. Lett. **87**, 052301 (2001).
- [8] Q.H. Zhang, V. Topor Pop, S. Jeon, and C. Gale, Phys. Rev. C **66**, 014909 (2002).
- [9] S. Jeon and S. Pratt, Phys. Rev. C **65**, 044902 (2002).
- [10] VENUS Collaboration, K. Werner, Phys. Rep. **232**, 87 (1993).
- [11] HSD Collaboration, W. Cassing and S. Juchem, Nucl. Phys. **A672**, 417 (2000).
- [12] ART Collaboration, B.A. Li and C.M. Ko, Phys. Rev. C **52**, 2037 (1995).
- [13] NEXUS Collaboration, H.J. Drescher, M. Hladik, K. Werner, and S. Ostapchenko, Nucl. Phys. B, Proc. Suppl. **75A**, 275 (1999).
- [14] S.E. Vance and M. Gyulassy, Phys. Rev. Lett. **83**, 1735 (1999).
- [15] URQMD Collaboration, S.A. Bass, M. Belkacem, M. Bleicher, M. Brandstetter, L. Bravina, C. Ernst, L. Gerland, M. Hofmann, S. Hofmann, J. Konopka, G. Mao, L. Neise, S. Soff, C. Spieles, H. Weber, L.A. Winckelmann, H. Stöcker, W. Greiner, C. Hartnack, J. Aichelin, and N. Amelin, Phys. Rev. Lett. **41**, 225 (1998).
- [16] AMPT Collaboration, B. Zhang, C.M. Ko, B.A. Li, and Z. Lin, Phys. Rev. C **61**, 067901 (2000).
- [17] For string fragmentation combined with hadronic cascade, See JPCIAE Collaboration, Sa Ben-Hao, Tai An, Wang Hui, and Liu Feng-He, Phys. Rev. C **59**, 2728 (1999).
- [18] QGSM Collaboration, N.S. Amelin *et al.*, Phys. Rev. D **46**, 4873 (1992).
- [19] For partonic cascade with hadronic cascade see, VNI/URQMD Collaboration, S.A. Bass, M. Hofmann, M. Bleicher, L. Bravina, E. Zabrodin, H. Stöcker, and W. Greiner, Phys. Rev. C **60**, 021901 (1999).
- [20] P. Bozek, W. Broniowski, and W. Florkowski, nucl-th/0310062.
- [21] B. Tomásik, Proceedings of 38th Rencontres de Moriond on QCD and High-Energy Hadronic Interactions, Les Arcs, Savoie, France, 2003 (to be published), nucl-th/0304079.
- [22] B. Tomásik, U.A. Wiedemann, and U. Heinz, Heavy Ion Phys. **17**, 105 (2003).
- [23] P. Siemens and J. Rasmussen, Phys. Rev. Lett. **42**, 880 (1979).
- [24] S. Pratt, Phys. Rev. Lett. **53**, 1219 (1984).
- [25] F. Retiere, Proceedings of the International Workshop on Physics of the Quark-Gluon Plasma, Palaiseau, France 2001, nucl-ex/0111013.
- [26] Particle Data Group, K. Hagiwara *et al.*, Phys. Rev. D **66**, 010001 (2002).
- [27] K.C. Chase and A.Z. Mekjian, Phys. Rev. C **52**, R2339 (1995).
- [28] S. Das Gupta and A.Z. Mekjian, Phys. Rev. C **57**, 1361 (1998).
- [29] S. Pratt and S. Das Gupta, Phys. Rev. C **62**, 044603 (2000).
- [30] S. Pratt, Phys. Rev. Lett. **84**, 4255 (2000).
- [31] S. Cheng and S. Pratt, Phys. Rev. C **67**, 044904 (2003).
- [32] S. Pratt and J. Ruppert, Phys. Rev. C **68**, 024904 (2003).
- [33] S. Pratt and S. Petriconi, Phys. Rev. C **68**, 054901 (2003).
- [34] M. A. Pichowsky, A. Szczepaniak, and J.T. Londergan, Phys. Rev. D **64**, 036009 (2001).
- [35] R. Kaminiski, L. Lesniak, and K. Rybicki, Acta Phys. Pol. B **31**, 895 (2000).
- [36] G. Grayer *et al.*, Nucl. Phys. **B75**, 189 (1974).
- [37] L. Rosselet *et al.*, Phys. Rev. D **15**, 574 (1977).
- [38] V. Shrinivasan *et al.*, Phys. Rev. D **12**, 681 (1975).
- [39] M. Kermani *et al.*, Phys. Rev. C **58**, 3431 (1998).
- [40] M.J. Losty, V. Chaloupka, A. Ferrando, L. Montanet, E. Paul, D. Yaffe, A. Zieminski, J. Alitti, B. Gandois, and J. Louie, Nucl. Phys. **B69**, 185 (1974).
- [41] P. Estabrooks and A.D. Martin, Nucl. Phys. **B79**, 301 (1974).
- [42] P. Braun-Munzinger, D. Magestro, K. Redlich, and J. Stachel, Phys. Lett. B **518**, 41 (2001).